Parametric Instability of Helical Oscillations with External Signals in a Positive Column.

Hiroshi SATOH, Masahiro ISHIKAWA, Yohko SHIRASAWA
Faculty of Textile Science and Technology, Shinshu University,
and
Michio MATSUMOTO
Faculty of Engineering, Yamanashi University.

1. Introduction

A long positive column plasma becomes unstable and chaotic, increasing longitudinal magnetic fields $\boldsymbol{B}$ beyond a certain critical field B_c. And the loss of charged particles across the fields $\boldsymbol{B}$ anomalously increases. This anomalous increase was found by Lehnert [1], and its physical mechanism was fundamentally explained by the helical instabilities [2], [3]. Since then, many papers on the diffusion phenomena due to those helical instabilities have been published theoretically [4-6] and experimentally [7-9].

While, another oscillations in the positive column, i. e. moving striations also were investigated by many workers [10-12]. Since a artificially controlling method for the moving striations were proposed by Wojaczek [13], the study on the striations were made rapidly to progress. Ohe and Takeda [14] searched out the dispersion relation of externally excited striations without the fields $\boldsymbol{B}$. Extending Keen's theory [15], they also analysised a synchronized phenomenon which is observed between external signals and self-excited striations. Suganomata et al have experimentally investigated about the frequency couplings between externally applied signals and ionization waves in SF_6 positive column [16], and given some mathematical analysis to them using Mathieu function [17].

We report here on the synchronized phenomena which arise between externally applied signals and helical waves, and discuss them in a method of parametric frequency coupling.

2. Analysis

We first give an analysis of the frequency coupling of excited waves with the externally applied signals. Next, we explain qualitatively the frequency synchronization.

We start with the following equations of density continuity and momentum

conservation for j-type particle (j=i for ion and =e for electron) which are derived for the Boltzmann equation on the assumptions of slow density variations and steady particle flows.

$$0=\frac{\partial n_j}{\partial t}+\nabla\cdot\boldsymbol{\Gamma}_j-\zeta n_e \quad \cdots\cdots(1)$$

$$0=-D_j\nabla n_j\pm\mu_j n_j\boldsymbol{E}\pm S_j(\boldsymbol{\Gamma}_j\times\boldsymbol{b})-\boldsymbol{\Gamma}_j \quad \cdots\cdots(2)$$

Where the $\boldsymbol{\Gamma}_j$ is the j-type particle flow density, ζ the particle production rate, $S_j=(\Omega_j\,\tau_j)$, Ω_j being the Larmor frequency and τ_j the mean collision time, and $\boldsymbol{b}$ the unit vector parallel to $\boldsymbol{B}$. In eq. (2) the upper sign is for ion and the lower for electron. From the solutions in steady state to eq.(1), the density $n_0(r)$ and potential $V_0(r)$ can be given by the usual forms [1].

When the external signal $E_1\cos\omega_s t$ is applied, the steady state density and potential suffer perturbations, which are expressed as $n=n_0+n'$ and $V=V_0+V'$. Here, we assume the perturbations to be small and the quasi-neutrality still maintained. The perturbation forms for the m=0 mode are prescribed as

$$n'=\tilde{N}(z,\,t)\,J_0(\beta_0 r) \text{ and } V'=\tilde{V}(z,\,t)\,J_0(\beta_0 r) \quad \cdots\cdots(3)$$

Where $\beta_0=\lambda_0/R$, R being the tube radius and $\lambda_0=2.4048$ the first zero point of the zeroth order Bessel function. Using eq. (3), eq. (1) yields in linear approximation as follows:

$$0=\{\frac{\partial}{\partial t}+i\,\mathrm{k}\mu_i\,(E_0+E_1\cos\omega_s t)\}\,J_0(\beta_0 r)\,\frac{\tilde{N}_\mathrm{k}(t)}{N_0}$$
$$+\mu_i\{\{\frac{\beta_0^2}{1+S_i^2}+\mathrm{k}^2\}\,J_0^2(\beta_0 r)-\frac{1}{1+S_i^2}(\frac{\partial J_0}{\partial r})^2\}\,\tilde{V}_\mathrm{k}(t) \quad \cdots\cdots(4)$$

Here, the E_0 is the discharge electric field, $\tilde{N}_\mathrm{k}(t)$ and $\tilde{V}_\mathrm{k}(t)$ are the Fourie transforms to the corresponding quantities and k is wave number. Assuming the plasma quasi-neutrality as mentioned above, the difference between the continuity equations (1) for ions and electrons leads to

$$0=\nabla\cdot(\boldsymbol{\Gamma}_i-\boldsymbol{\Gamma}_e)$$
$$=\{-\mathrm{k}^2D_e+i\mathrm{k}R\mu_e(E_0+E_1\cos\omega_s t)\}\,J_0(\beta_0 r)\,\frac{\tilde{N}_\mathrm{k}(t)}{N_0}$$
$$+\mu_e\{\frac{1+S_iS_e}{1+S_e^2}\beta_0^2+\mathrm{k}^2\}\,J_0^2(B_0 r)-\frac{1+S_iS_e}{1+S_e^2}(\frac{\partial J_0}{\partial r})^2\}\,\tilde{V}_\mathrm{k}(t) \quad \cdots\cdots(5)$$

We make the operation $\int_0^R dr\,r\,J_0(\beta_0 r)$ apply to eqs. (4) and (5), to remove the r-dependence, and eliminate $\tilde{V}_\mathrm{k}(t)$ from those equations obtained, in a approximation $(S_e\mathrm{k}R)^2\ll 1$ for the strong fields $\boldsymbol{B}$, we obtain

$$0=\frac{i}{\Pi}\,\frac{\partial\tilde{N}_\mathrm{k}}{\partial t}+\{\frac{\alpha}{\mathrm{k}R}(1+\epsilon\cos\omega_s t)+i\frac{D_e}{\mu_e RE_0}\{\alpha+(\mathrm{k}R)^2\}\}\,\tilde{N}_\mathrm{k}(t) \quad \cdots\cdots(6)$$

Here, $\Pi=\mu_i E_0/R$ is the frequency for the normalization, $\varepsilon=E_1/E_0$ and $\alpha=2.89$ from the r-integration.

By Fourier transformation $x(\omega)=\int_{-\infty}^{\infty}dt\, e^{i\omega t}\tilde{N}_k(t)$, eq. (6) follows

$$\left[\omega+\alpha\frac{\Pi}{kR}+i\eta\{\alpha+(kR)^2\}\right]x(\omega)=-\alpha\frac{\Pi}{kR}\frac{\varepsilon}{2}\{x(\omega+\omega_s)+x(\omega-\omega_s)\}\cdots(7)$$

Here, $\eta=D_e/\mu_e RE_0$ is a small value in our experiment. The right hand side denotes an effect of the external signals. When $\varepsilon=0$, we obtain $\omega=-\alpha\Pi/(kR)-i\eta\cdot\{\alpha+(kR)^2\}$ for kR not so small. This is a dispersion form for the backward ionization wave.

We take $\Omega_0=-\alpha\Pi/kR$ for an eigen-frequency of the positive column plasma within the uniform region of $\boldsymbol{B}$. In eq. (7) we have the frequency coupling between $x(\omega)$ and $x(\omega-\omega_s)$ for the external frequency $\omega_s(\simeq 2\Omega_0)$ and the excited wave frequency ω $(\simeq\Omega)$.

$$G(\omega-\omega_s)\,x(\omega-\omega_s)=-\frac{\varepsilon}{2}\Omega_0\,x(\omega)\quad\cdots\cdots(8)$$

where $G(\omega)=\omega+\Omega_0+i\eta\{\alpha+(kR)^2\}$ for simplicity. In a resonant approximation, the above equation (7) with eq. (8) comes to $G(\omega)\cdot G(\omega-\omega_s)\simeq(\varepsilon^2/4)\Omega_0$, which yields

$$\omega\simeq\pm\Omega_0\sqrt{1+\varepsilon^2/4}-i\eta\{\alpha+(kR)^2\}\quad\cdots\cdots(9)$$

This is the frequency for the $m=0$ mode wave coupled with the signal $(\omega_s\simeq 2\Omega_0)$. The second term indicates the damping due to the particle diffusion. Therefore, some appropriate amplitudes of the signals are required to excite the wave.

Next we derive a dispersion relation for the helical wave, and explain qualitatively the frequency synchronization. In this case, the perturbations are supposed as

$$n'=\tilde{N}J_1(\beta_1 r)\,e^{-i\omega t+im\theta+ikz}+c.c\quad\cdots\cdots(10)$$
$$v'=\tilde{V}J_1(\beta_1 r)\,e^{-i\omega t+im\theta+ikz}+c.c$$

Here, $m=1$ or -1 and $\beta_1=\lambda_1/R$, $\lambda_1=3.832$ being the first zero point of the first order Bessel function. Using the similar calculation method as before, we obtain the following dispersion relation,

$$\Omega=kR+\frac{\eta}{1+\delta S_e^2}(\alpha_2 S_i+i\alpha_1)-\eta(\lambda_1^2-\alpha_3+\alpha_4(kR)^2-iS_i\alpha_5).$$
$$\frac{\dfrac{1+S_e^2}{\eta}kR-\dfrac{\alpha^2 S_e}{1+\delta S_e^2}i\{(\lambda_1^2-\lambda_0)^2+\alpha_1+(1+S_e^2)(kR)^2\}}{(1+S_e^2)(\lambda_1^2+\alpha_4+\alpha_3)+\alpha_4(1+S_e^2)(kR)^2+i\alpha_5 S_e}\quad\cdots\cdots(11)$$

Here, $\delta=\mu_i/\mu_e$, $\alpha_1=-2.827$, $\alpha_2=-4.326$, $\alpha_3=1.700$, $\alpha_4=0.588$ and $\alpha_5=-2.264$, $\alpha_n(n=1\sim5)$ are from the r-integration. The results of eq. (11) are graphically shown in Fig. 6. The growth rates $\gamma=I_m(\Omega)$ increase sensitively as the increase of the fields $\boldsymbol{B}$. From curves for $\gamma<0$, we can deduced that the helical wave will be excited synchronizingly by the externally supplied signals with some appropriate amplitudes

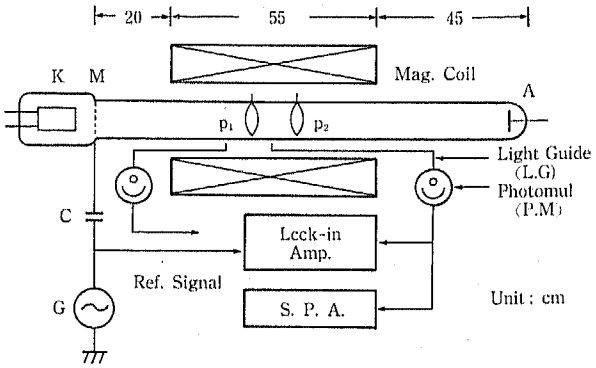

Fig. 1 Experimental arrengement.

and frequencies.

3. Experimental Apparatus and Measurement

An arrangement of the present experiments is schematically shown in Fig. 1. A hot cathode-discharge tube is of 150 cm in length and of 1.5 cm in radius. The discharge tube is placed in and parallel to the axis of a solenoidal coil which is of 5 cm in inside diameter and of 55 cm in length. The magnetic fields $\boldsymbol{B}$ are uniform along about 30 cm in the middle part of the coil. The coil is located close to the cathode of the tube, because the externally applied signals can propagate only in a relatively short distance. The base pressure of 5×10^{-7} Torr before injecting He-gas into the tube was obtained by using a liquid nitrogen trap. The external signals are supplied by mesh-electrode (M) which is through a condenser (C) inserted in series to a sine wave generator (G), which gives a root mean square value 20V as an external signal's source. By two photomultipliers (P. M), light signals coming out from the positive column are detected. One of the two P. M is fixed and the other can be moved parallel to the tube axis, and also moved in the azimuthal direction. The waves detected by the P. M are represented on the synchroscope, and are analyzed by a spectrum analyzer noted as "S. P. A" in Fig. 1. Since the amplitudes of the waves are generally very small, they are mainly measured by a lock-in amplifier. The resolving power of the lock-in amplifier is less than about 0.3 rad. Probes P_1 and P_2 are the ring ones located 2 mm inside around the tube wall, which are used for the measurement of time-averaged axial fields. The measurements are made in the range of discharge currents $I_p=(50\text{-}200)$ mA and of gas pressures $P=(0.2\text{-}0.6)$ Torr. The fields $\boldsymbol{B}$ are changed over the range $B=(0.0\text{-}1.2)$ KG.

4. Experimental Results

We first make experimentally research on the dispersion relation and the

synchronization of the parametrically excited waves, and next compare those results with analytical ones.

4.1 Parametric Excitation of Helical waves

When the fields $\boldsymbol{B}$ are much less than a critical field B_c, frequency spectrum of the externally excited waves in the positive column consists of the applied signal and its harmonic components, and they have all the character of $m=0$ mode waves. In the fields $\boldsymbol{B}$ slightly less than B_c, helical waves in addition to the $m=0$ mode can be abruptly excited only by supplying the external signals with some appropriate amplitudes and frequencies. The typical spectrum of them is shown in Fig. 2 for case of gas pressure P=0.3 Torr, B=0.9 KG ($<B_c=0.94$ KG) and the signal's frequency $f_s=20$ KHz. The figure shows the excitation of four waves which have respectively 1/2, 2/2, 3/2 and 4/2 times of the signal's frequency f_s. And their modes are the $m=0$ for the two waves of $(\frac{1}{2}f_s)$ and $(\frac{3}{2}f_s)$, $m=1$ for $(\frac{2}{2}f_s)$ and $m=2$ for the rest. These four waves are also excited in the same character by the signal with $f_s=10$, 30 or 40 KHz. Such external excitations are observed in the field range of $0.7\,B_c \lesssim B \lesssim B_c$ for P=0.3 Torr. The excitations of the above waves may be considered due to a parametric frequency coupling.

The amplitudes and frequencies of the externally excited waves change synchronously with the frequency of applying signal. The synchronizations occur at each $f_s=(\frac{n}{2}f_h)$, (n=1, 2, 3 and 4). Here, the f_h are frequencies of excited helical wave $m=1$ mode.

Figure 3 shows amplitudes of the external signal which is required to the excitation of the $m=1$ mode wave (growth rate), at some frequencies and fields B,

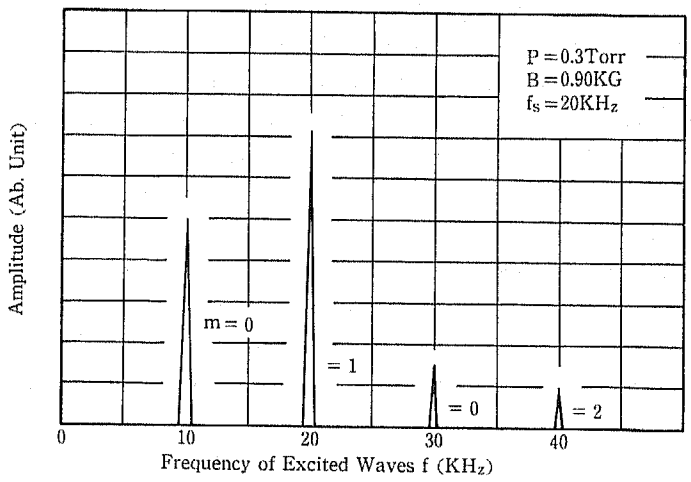

Fig. 2 Frequency spectrum of externally excited waves.

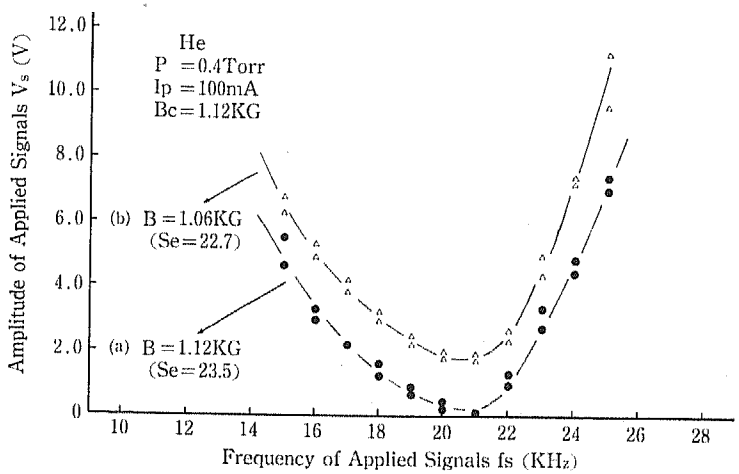

Fig. 3 Amplitudes of external signal required to excitation of m=1 mode wave.

i. e. shows that the $m=1$ mode wave become hard to excite with decrease of the fields $\boldsymbol{B}$. Asymmetries of the growth rate to the f_s may be due to a shift of an excitation position on the z-axis of the $m=1$ mode wave, which depends on f_s. In our experiments, as this position is shifted to the anode side with the increase of f_s, the wave length of the $m=1$ wave which is determined by the system is considered effectively becoming short.

4.2 Synchronization at $B \gtrsim B_c$

The above synchronization is also observed between the external signals and self-excited helical waves at $B \gtrsim B_c$. As the external signals with frequencies f_s are applied to the helical wave $m=1$ mode with frequency f_h which is already excited at the fields $\boldsymbol{B}$ ($\gtrsim B_c$), the f_h of $m=1$ mode wave changes synchronously with f_s over a certain frequency range. As a typical example, we show the case of P=0.4 Torr, B=1.05 KG ($>B_c=1.03$ KG) in Fig. 4 (a~d). Figure 4 (a) shows that for $f_s \ll f_h$ the helical wave $m=1$ mode is independent of the external signals and a beat frequency $|f_s-f_h|$ is observed. As increasing f_s and approaching to a certain value less than f_h, the helical wave frequency f_h is suddenly pulled in that value of f_s and the $m=1$ mode wave only is remained, as shown in Fig. 4 (b). The helical wave frequency f_h increases synchronously with the increase of f_s as shown in Fig. 4 (b) and (c). This synchronization occurs in a frequency range of $(f_h-\Delta f_s) \lesssim f_s \lesssim (f_h+2\Delta f_s)$, where $f_h=26$ KHz and $\Delta f_s \simeq 3.2$ KHz. When the f_s exceeds that range, the helical wave becomes independent of the signals and the beat frequency appears again, as shown in Fig. 4 (d). The synchronizations also slightly occur in the narrow ranges for each $f_s=(\frac{n}{2} f_h)$ (n=1, 3, 4). Amplitudes of the $m=1$ mode within the synchronization range have the

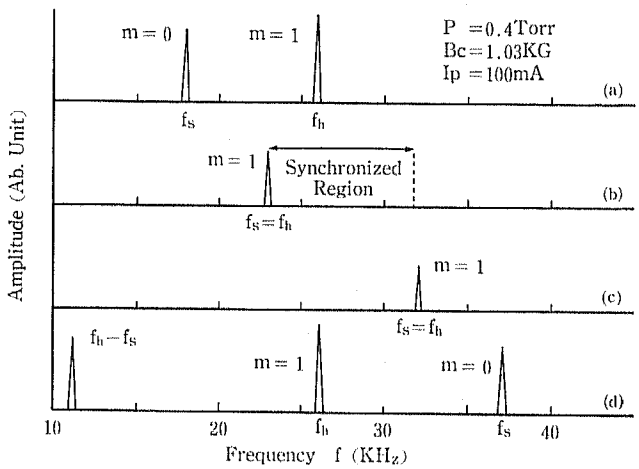

Fig. 4 Synchronized phenomena between external signals and self-excited wave (m=1 mode).

maximum value at $f_s = f_h$, and becomes larger than that of the self-excited $m=1$ mode itself. This means that the growth rate of the $m=1$ mode is further increased by the supply of the external signals.

4.3 Dispersion Relations of Excited m=1 mode

We investigate the character of the externally excited waves at the fields $\boldsymbol{B}$ less than the critical field B_c. Figure 5 shows the dispersion curves for the excited waves at some values of the fields $\boldsymbol{B}$ for P=0.3 Torr and $I_p = 100$ mA. In this case, $B_c =$ 0.94 KG. Curve (a) is for B=0. The upper branch with negative slope of the wave (f $\gtrsim$18 KHz) for the mode $m=0$ is indicative of the character of ionization waves,

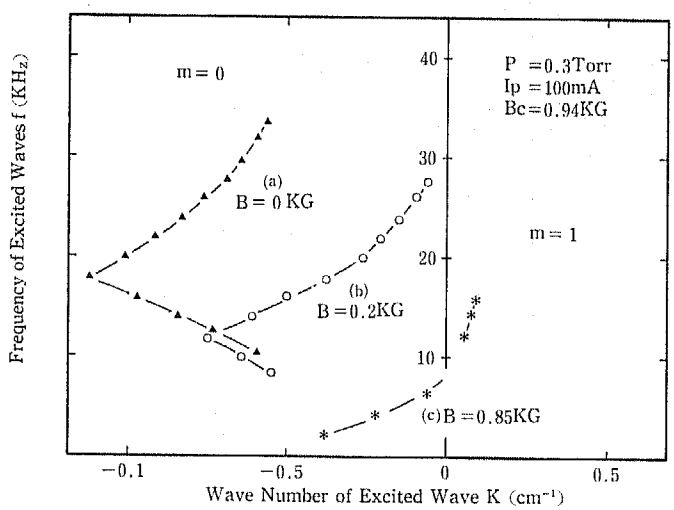

Fig. 5 Dispersion relations of externally excited waves at $B < B_c$.

which is approximately described by empirical relation $kf=const.$ The lower branch with positive slope does of ion acoustic waves, which is approximately described by $f/k=C_s$. Here, the C_s is ion acoustic velocity. This curve is consistent in tendency with Ohe and Takeda's results [14] by a current modulation methods. Curve (b) is for $B=0.2$ KG, the range for ion acoustic waves become narrow, and an inflection point from ion acoustic to ionization waves shifts to the lower frequencies. Curve (c) is for $B=0.85$ KG. Here, the branch for the ion acoustic waves does not exist, and another branch for the helical wave $m=1$ mode does newly. Namely as increasing the external signal's frequency f_s at $B=0.85$ KG, the excited waves of the $m=0$ mode becomes gradually weak in amplitude and negligible at $f_s \simeq 9.6$ KHz. Further increasing f_s, the helical wave of the $m=1$ mode insted of the $m=0$ mode is excited and growing. Such a mode conversion synchronized with the external signals is observed in the fields $B=(0.7\sim0.94)$ KG.

The process of the mode conversion at $B<B_c$ is as follows. When the external signals of low frequencies are supplied, the excited wave has a character of the axially symmetric $m=0$ mode. With increasing the signal's frequencies f_s, the wave plane starts inclining to the tube axis and twisting in the direction of ion's gyration, i. e. of the helical wave $m=1$ mode. As further increasing f_s, above tendency becomes remarkable, and when the wave length of the $m=0$ mode becomes the

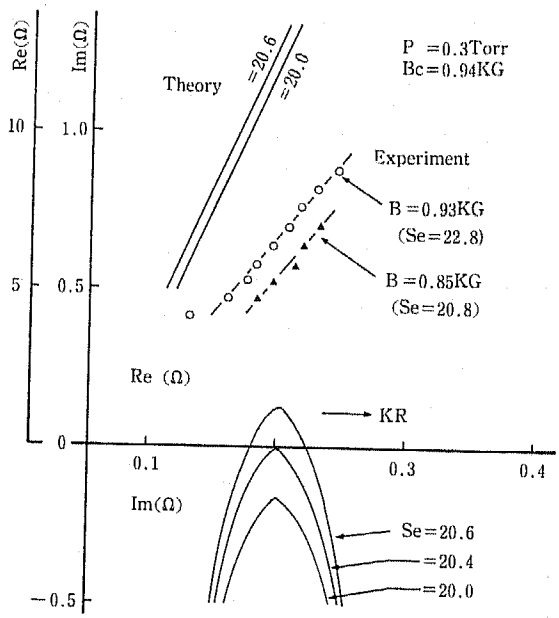

Fig. 6 Experimental and theoretical dispersion reations of excited waves ($m=1$ mode) in gas pressure $P=0.3$ Torr at $B<B_c$.

longest, the mode conversion from the $m=0$ to the $m=1$ occurs suddenly (see Fig. 4 (c)).

Then we show graphically a dispersion relation for the helical wave $m=1$ mode in Fig. 6 and explain qualitatively the frequency synchronization. Curve (a) indicates the experimental results of the dispersion relation, and Curves (b) and (c) do the analytical results of the dispersion relation and growth rate for the $m=1$ mode, respectively. The growth rates $\gamma=\mathrm{Im}(\omega)$ increases sensitively as the increase of $\boldsymbol{B}$. From the curve for $\gamma<0$, we can deduce that the herical wave will be excited synchronizingly by the externally supplied signal with some appropriate amplitudes and frequencies.

5. Conclusion

The excitaion of the helical wave is considered due to the difference of ion-and electron-flows in the azimuthal direction. Therefore, the externally excited helical wave at $B<B_c$ is also excited by applying some appropriate disturbances e.g. by disturbing the magnetic flux of the cathode side with iron pieces instead of the above sine wave. This excitation is due to the parametric frequency coupling. As seen in Fig. 6 when the external signal with a frequency f_s is applied in the positive column plasma, the helical wave $m=1$ mode of the corresponding wave number k is excited only one. The external synchronization at $B>B_c$ are explained by the same reason as above.

References

[1] B. LEHNERT : Proc. of the 2nd Int. Conf., **32**, 349, 1958.
[2] B. B. KADOMTSEV and V. NEDOSPASOV : J. Nucl. Energy C1, **230**, 1960.
[3] F. C. HOH : Phys. Fluids, **5**, 22, 1962.
[4] G. V. GIERKE and K. H. WöHLER : Nucl. Fusion Supplement Part **147**, 1962.
[5] G. JANZEN, F. MOSER and E.RAUCHLE : Z. Naturforsch **25a** 992, 1970.
[6] Φ. HOLTER and R. R. JOHNSON : Phys. Fluids, **8**, 333, 1965.
[7] F. C. HOH and B. LEHNERT : Phys. Fluids, **3**, 833, 1960.
[8] G. A. PAULIKAS and R. V. PYLE : Phys. Fluids, **5**, 348, 1962.
[9] M. SATO and Y. HATTA : Appl. Phys. Letters, **9**, 423, 1966.
[10] W. PUPP : Phys. Z., **33**, 844, 1932.
[11] W. PUPP : Phys. Z., **36**, 61, 1935.
[12] H. YOSHIMOTO and Y. YAMASHITA : J. Phys. Soc. Japan, **16**, 1649, 1961.
[13] K. WOJACZEK : Ann. Phys. **2**, 68, 1965.
[14] K. OHE and S. TAKEDA : Japaneas J. Appl. Phys., **11**, 1173, 1972.
[15] B. E. KEEN : Phys. Rev. Letter **24**, 260, 1970.
[16] I. ISHIKAWA, M. MATSUMOTO and S. SUGANOMATA : J. Phys. D : Appl. Phys., **17**, 85, 1984.

[17] S. SUGANOMATA, I. ISHIKAWA, Y. MATSUOKA and M. MATSUMOTO : J. Phys. D : Appl. Phys., **17**, 1984.